The Detectability Limit of Organic Molecules within Mars South Polar Laboratory Analogues

Jacqueline D Campbell, B Schmitt, O. Brissaud, J.-P. Muller

HAL Id: hal-03309251
https://hal.science/hal-03309251

Submitted on 30 Jul 2021

1

The Detectability Limit of Organic Molecules within Mars South Polar Laboratory Analogues

J. D. Campbell [1,2], B. Schmitt [3], O. Brissaud [3], J-P. Muller [1]

[1] Imaging Group, Mullard Space Science Laboratory, Department of Space and Climate Physics, University College London (UCL), Holmbury St. Mary, RH5 6NT, UK

[2] now at Dept. of Earth Sciences, University of Oxford, OX1 3AN, UK

[3] Université Grenoble Alpes, CNRS, Institut de Planétologie et d'Astrophysique de Grenoble, France

Corresponding author: Jacqueline D. Campbell (jacqueline.campbell@earth.ox.ac.uk)

11

Key Points:

- A new spectrum diagnostic of Polycyclic Aromatic Hydrocarbons (PAHs) pertinent to Mars has been produced

- The detectability limit of PAHs in Mars South Pole analogues has been established

- The evolution of the spectra of PAHs in Mars South Pole analogues as ice sublimates under emulated Martian conditions has been recorded

20 **Abstract**

21 A series of laboratory experiments was carried out in order to generate a diagnostic spectrum for
22 Polycyclic Aromatic Hydrocarbons (PAHs) of astrobiological interest in the context of the
23 Martian South Polar Residual Cap (SPRC), to establish PAH spectral features more easily
24 detectable in CO_2 ice (mixed with small amounts of H_2O ice) than the previously reported
25 absorption feature at 3.29 µm in order to constrain their detectability limit. There is currently no
26 existing literature on PAH detection within SPRC features, making this work novel and
27 impactful given the recent discovery of a possible subglacial lake beneath the Martian South
28 Pole. Although they have been detected in Martian meteorites, PAHs have not been detected yet
29 on Mars, possibly due to the deleterious effects of ultraviolet radiation on the surface of the
30 planet. SPRC features may provide protection to fragile molecules, and this work seeks to
31 provide laboratory data to improve interpretation of orbital remote sensing spectroscopic
32 imaging data. We also ascertain the effect of CO_2 ice sublimation on organic spectra, as well as
33 provide PAH reference spectra in mixtures relevant to Mars. A detectability limit of ~0.04% has
34 been recorded for observing PAHs in CO_2 ice using laboratory instrument parameters emulating
35 those of the Compact Reconnaissance Imaging Spectrometer for Mars (CRISM), with new
36 spectral slope features revealed between 0.7 and 1.1 µm, and absorption features at 1.14 and,
37 most sensitively, at 1.685 µm. Mars regolith analogue mixed with a concentration of 1.5% PAHs
38 resulted in no discernible organic spectral features. These detectability limits measured in the
39 laboratory are discussed and extrapolated to the effective conditions on the Mars South Polar
40 Cap in terms of dust and water ice abundance and CO_2 ice grain size for both the main perennial
41 cap and the H_2O ice-dust sublimation lag deposit.

42 **Plain Language Summary**

43 Carbon molecule chains, or organics, are considered important in the search for life, as all life
44 that we know of on Earth is made from carbon. A particular type of organic, PAHs, that are
45 really common on Earth and throughout space, have never been found on Mars and it is likely
46 they are broken down too quickly on the Martian surface by the Sun's radiation to be discovered
47 using space satellites. However, some areas of Mars move and change, and expose dust. One
48 such area is the Martian South Polar Cap. This study uses laboratory experiments to simulate
49 expected conditions on the Mars South Pole, and mix PAHs with ices, then look at them using
50 instruments similar to those on satellites orbiting Mars to find out how much PAH material
51 would have to be in the ice to be able to detect it. These experiments allowed us to create a
52 spectrum that can be used to help to identify different materials. We have found that you can
53 observe features of PAHs at 1.685 and 1.14 µm in the spectra when there is 0.1% or more PAH
54 in a carbon dioxide ice sample, but it was not possible to see 1.5% of PAH in a sample of dust
55 similar to the dust on the surface of Mars.

56 **1 Introduction**

57 Our neighbouring planet, Mars, has increasingly been the target of scientific exploration and of
58 particular interest are its geological history, current environmental conditions, and perhaps most
59 importantly, its potential as a host for extraterrestrial life (Fairén et al., 2010). The polar caps of
60 Mars have more recently emerged as an area of scientific interest due to their abundance of water
61 ice and their dynamic nature, especially with the discovery of a possible stable body of liquid
62 water beneath the Martian South Pole (Orosei et al., 2018). The Martian North and South Pole

63 have permanent ice caps that expand throughout their respective winters, and maintain residual
64 caps in the summer. The North Polar Cap (NPC) is composed almost entirely of water ice, while
65 the longer, colder winter in the higher altitude southern hemisphere means that the central part of
66 the South Polar Cap (SPC) is covered by a permanent layer of CO_2 ice (Byrne, 2009), up to 10
67 metres thick, underlain, and surrounded by, water ice layers known as Polar Layered Deposits
68 (PLD; Piqueux et al., 2008).

69 Seasonal cycles of sublimation and deposition of CO_2 ice on the SPC are responsible for the
70 formation of 'Swiss Cheese Terrain' (SCT). This unique cryomorphology manifests as flat-
71 topped mesas with flat floored, quasi-circular depressions that form patterns resembling
72 Emmental Swiss Cheese (Malin et al., 2001). This terrain forms by preferential and progressive
73 sublimation and erosion of the walls of the depressions, at a typical speed of 3 metres per Mars
74 year. The reason these SCT sublimations features are of interest to this study is because of the
75 exposure of dust previously shielded within the SPC (Jian et al., 2009). The exposed dust that
76 has been concentrated by CO_2 ice sublimation may be a candidate site for the detection of a class
77 of organic molecules, Polycyclic Aromatic Hydrocarbons (PAHs), that may have been protected
78 from the Sun's radiation within the SPC. If PAH is dispersed in the ice instead of being
79 associated with the dust, it will also be concentrated at the surface with the dust as the ice
80 sublimates away leaving any particles behind.

81 Work was previously carried out in order to look for PAH signatures on the thin, dust-covered
82 rims of SCT to no avail (Campbell et al., 2018) using the well-known PAH diagnostic absorption
83 feature at 3.29 µm (Allamandola, 2011), but no signs of PAHs were found. However, this strong
84 band is situated in the high wavelength wing of the very strong 3.1µm band of water ice and may
85 thus be hidden in places where abundant water ice is present, such as on SPC margins (Douté et
86 al. 2007) and rim scarps (Campbell at al., 2018). It may be also hidden by the wide hydration
87 bands of minerals (adsorbed and structural water) that can extend up to 4 µm and may even be
88 saturated in some cases.

89 The aims of the experiments carried out and reported here were to generate a diagnostic near-
90 infrared spectrum for PAHs of astrobiological interest in the context of the Martian South Pole.
91 We emulate the parameters of the CRISM instrument's Full Resolution Targeted (FRT) ~18
92 m/pixel mode to constrain the detectability limit of PAHs in CO_2 ice to establish the
93 characteristics of PAH spectral features at wavelengths other than the absorption feature at 3.29
94 µm, where they might be easier to discern against the CO_2 and H_2O ice spectrum. In addition, we
95 discuss how the detectability of these bands is affected by the presence of dust.

96   1.1 Polycyclic Aromatic Hydrocarbons

97 PAHs are a group of chemical compounds consisting of benzene rings of carbon with hydrogen.
98 In its NPAH form, nitrogen can be substituted for carbon atoms in the aromatic ring (Tang,
99 2018). PAHs occur not only on Earth, but throughout the universe. They have been found to
100 coalesce in space within dust clouds (Mulas et al., 2005), and are thought to account for up to
101 20% of total cosmic carbon (Allamandola, 2011).

102 PAHs frozen within ice particles in dense molecular clouds in space undergo processing by
103 ultraviolet light and cosmic rays to produce more complex species (Dartnell et al., 2012). PAHs

104   can also arise and increase in abundance through the irradiation of complex polymeric organic

105   material such as those found in carbonaceous meteorites (Thompson et al., 2020). A recent

106   paper on the Mukundpura carbonaceous chondrite meteorite found in India measured 500ppm

107   PAH (Kalpana et al., 2021). PAHs eventually rain down on primordial planets directly from

108   planetary accretion discs, or are delivered on comets and meteorites (Allamandola, 2011).

109   Therefore, PAHs should be present, or should have been present in the past, on all planetary

110   bodies in the solar system (Dullemond et al., 2007). PAHs have been detected on the surfaces of

111   Saturnian icy moons and comets (Cruikshank et al., 2008, 2014; Lopez-Puertas et al., 2013; Li,

112   2008) and have been measured in other carbonaceous chondrites meteorites at the level of a few

113   ppm (Becker at al. 1997).

114   The delivery of complex organic compounds to planets via bolide impact is a very important

115   concept in astrobiology, and could be instrumental in explaining abiogenesis (the origin of life).

116   Carbon's propensity to catenate (form long chains), and the carbon-based nature of all life on

117   Earth, means that the presence of carbon compounds is considered an essential component of any

118   potentially habitable environment (Plaxco and Gross, 2011). PAHs are sought after on many

119   solar system bodies in the search for the origin of life, but are conspicuously missing on Mars

120   (Benner et al., 2000). The discovery of PAHs on Mars would tell us that these organics could

121   survive in oxidizing environments receiving high levels of UV radiation, and may have

122   accumulated in the past when Mars had warmer and wetter conditions favourable to the

123   emergence of life.

124   1.2. PAHs on Mars

125   The detection of organics has been a primary objective of orbiters and landers since the Viking

126   missions (Klein, 1978). Despite apparent negative results for the detection of extant life by the

127   Viking landers in the 1970s, which searched for traces of biologically important compounds

128   (Klein, 1978; Schuerger and Clark, 2008), perchlorates were discovered by the 2008 Phoenix

129   lander (Hecht et al., 2009). More recently, organics were discovered by the Sample Analysis at

130   Mars (SAM) instrument on NASA's 2012 rover mission, Mars Science Laboratory (Freissinet et

131   al., 2015), known as "Curiosity". Perhaps of even more interest, is the re-analysis of the 1976

132   Viking Lander data by Navarro-Gonzalez et al. (2010) using modern laboratory techniques

133   suggested that there were both perchlorates and organic carbon present at the Viking Lander

134   sample sites, although they were not identified at the time. To date, no PAHs have been found on

135   Mars, but concentrations of about 1ppm of PAH have been found in Martian meteorites with

136   potential extraterrestrial origin (McKay et al. 1996, Becker at al., 1997; Botta and Bada, 2002).

137   A study by Dartnell et al. (2012) found that PAHs might be afforded protection from the effects

138   of UV radiation and oxidization within the subsurface of Mars, within rock, or in permanently

139   shadowed areas. Ice can also provide a barrier to deep UV solar radiation (Vincent, 1998;

140 Cockell et al., 2000), resulting in partial shielding and allowing organic compounds to become
141 more complex (Herbst and van Dishoek, 2009; Oberg et al., 2009).

142 **2 Laboratory Analysis**

143   2.1 Instruments

144   2.1.1. Laboratory Analysis

145 The site of the experiments was the Cold Surfaces Spectroscopy Facility (https://cold-
146 spectro.sshade.eu) at the Institut de Planétologie et d'Astrophysique de Grenoble (IPAG) in
147 France and has facilities for in-situ formation of ices, and cold rooms capable of keeping samples
148 up to -40°C to allow stable thermal conditions during preparation of icy materials for
149 experiments. This allows analysis of samples in the cryogenic CarboN-IR environmental cell,
150 which can maintain cold temperatures and low gas pressures, using the SHINE
151 (SpectropHotometer with variable INcidence and Emergence) instrument to record reflectance
152 spectra in visible and near-mid infrared wavelengths.

153   2.1.2. Spectro-gonio radiometer

154 The SHINE spectro-gonio radiometer was developed at IPAG, and is designed to measure
155 bidirectional reflectance and polarisation distribution functions of planetary material, enabling
156 the production of accurate datasets to help describe surface composition, roughness and texture
157 (Brissaud et al., 2004). In particular, the SHINE spectro-gonio radiometer is able to characterise
158 the light scattering properties of snows of various grain-size, compactness and surface roughness
159 at different stages of metamorphism. The instrument is able to measure from 0.35-4.80 μm, with
160 spectral resolution of between 6-40 nm, dependent on wavelength (ibid).

161 SHINE can be used in conjunction with the CarboN-IR environmental cell to analyse materials at
162 low temperatures.

163

164   2.1.3. CarboN-IR Environmental Cell

165 The CarboN-IR environmental cell system (https://cold-spectro.sshade.eu/carbo-nir-simulation-
166 chamber) allows for the study of planetary material samples in stable conditions. It can cool the
167 sample down to -210°C within an isothermal copper cell that can maintain a stable gas pressure
168 in thermodynamic equilibrium with the sample at the same temperature. The chamber is
169 designed to enable visible and near-IR monitoring throughout the physical evolution of ice
170 samples thanks to sapphire windows (Grisolle 2013).

171 **3 Methods**

172 The concept of this work is to produce empirical experimental data to support the interpretation
173 of data from orbital observations of the Martian SPC, namely the Compact Reconnaissance
174 Imaging Spectrometer for Mars (CRISM) on board NASA's Mars Reconnaissance Orbiter

175   (MRO), which has a surface spatial resolution of around ~18m/pixel (Murchie et al., 2007), with
176   a spectral resolution of ~6 nm.

3.1. Instrument parameters

178   The CRISM instrument has a resolution, of 9-19 nm full width at half maximum (FWHM) with
179   6.55 nm sampling over the 0.36-3.92 µm range (Murchie et al., 2007) In order to get a spectral
180   resolution as close as possible to CRISM, we recorded spectra over the 0.7-3.6 µm spectral range
181   using SHINE with a fixed slit of 1.5 mm, leading to 9-19 nm spectral resolution, and sampled
182   every 10 nm (except for the first experiment sampled at 20 nm). To complete a full reflectance
183   spectrum at this resolution took > 2.5 hours, so in order to effectively reduce the time between
184   two spectra, especially during ice sublimation, in many instances multiple shorter spectra at
185   wavelengths of interest were taken. The SHINE angular parameters used were fixed incidence
186   angle = 0°, and observation angle = 20°, optimized for the CarboN-IR cell. This is comparable
187   with a median phase angle of 0-30° for CRISM (Ceamanos et al., 2013).

3.2. Sample Preparation

189   Three samples were analysed for various ratios of PAHs mixed with CO_2 ice and two with finely
190   ground Martian simulant JSC-Mars 1 (Allen et al., 1998). Much of the existing literature on
191   PAHs found on icy moons and comets references the laboratory spectra recorded by Colangeli et
192   al., (1992), which is pertinent to PAHs of astrophysical interest, rather than astrobiological, or
193   specifically Martian. The six PAH species analysed by Colangeli et al., (1992) were benzene,
194   chrysene, triphenylene, perylene, benzo [a] pyrene, pentacene and coronene. While chrysene and
195   perylene have been found in Martian meteorites (Becker et al., 1997) and phenanthrene, pyrene,
196   chrysene, perylene or benzopyrene and anthanthracene were found by McKay et al. (1996) the
197   remaining four types of PAH have never been detected in Martian material. Therefore, we
198   analysed our own mixture of PAHs based on those identified by McKay et al. (1996) in the
199   ALH84001 and EETA79001 Martian meteorites but absent from Colangeli's analysis. The PAHs
200   used were an existing mixture of anthracene ($C_{14}H_{10}$), phenanthrene-d10 ($C_{14}D_{10}$), and pyrene
201   ($C_{16}H_{10}$) in raw form, obtained from Sigma-Aldrich (www.sigmaaldrich.com), in a 300 mg
202   sample of equal parts of each PAH species. We will not discuss in this paper the bands due to or
203   modified by the deuterated species as they do not contribute to PAH spectral features of interest.

204   In studies of Saturnian moons Iapetus and Phoebe (Cruikshank et al., 2008), the amount of PAHs
205   detected on the surface was 10^{-4} to 10^{-3} g/cm^3 (0.01-0.1 %) so the first sample used 0.10 % PAH
206   followed by 0.54 % and 0.67 % weight fractions for our three PAH samples mixed with CO_2 ice
207   in order to allow the detection limit to be determined by plotting band depth as a function of
208   concentration. The percentage amounts of PAH in CO_2 ice were difficult to fix precisely because
209   some CO_2 ice sublimated during the process of mixing the materials, but they were precisely
210   measured when the sample holder was filled with the prepared mixture, just before their
211   introduction into the cell (see below).   Increases in the amount of PAH for Samples 2 and 3 were
212   chosen based on how well we could see the PAH features in Sample 1.

213   CO_2 ice was obtained from liquid decompression with a commercial device SnowPack©. This
214   produces a granular snowpack of 312.5 cm^3 composed of small CO_2 ice grains. The average size
215   of the grains, 150 µm, was estimated by measuring the true surface of the grains observed with a

216 binocular microscope (Philippe et al. 2016). Part of the CO_2 ice snow pack was then manually
217 crushed, weighed, and a known mass of PAH powder was added and thoroughly mixed in a
218 stainless-steel container pre-cooled with liquid nitrogen to limit CO_2 ice sublimation. The cell,
219 also pre-cooled at -196°C, was filled up to its rim with the mixture (slightly compressed) and
220 weighed before rapid installation inside the pre-cooled CarboN-IR environment chamber (-100
221 °C). The Martian South Pole's lowest temperatures can reach -153 °C and never exceeds -60 °C
222 with the spring/summer temperatures for the SPC typically ranging between -80 and -100 °C
223 (Smith, 2004); hence the choice to keep the environmental cell at the lower spring/summer
224 temperature. The sapphire windows of the cryogenic chamber and of the external chamber were
225 then successively closed and air was completely evacuated from both volumes by pumping using
226 a detailed protocol developed to avoid frost condensation on the windows.

227 The grain sizes of our CO_2 ice samples are much smaller than what is generally observed on
228 Mars South Polar Cap where CO_2 ice tends to have very coarse centimeter sized grains, generally
229 in the form of compact slab (Douté et al. 2007). However, a major decrease in grain size, down
230 to the millimeter, occurs after equinox (Langevin et al. 2007) and corresponds to the large
231 increase of albedo oberved over the perennial cap during its sublimation phase. The grains in our
232 samples are typically 5-10 times smaller than during the polar cap sublimation phase of interest.
233 However, preparing such coarse grained CO_2 ice grains is a quite complex process and takes
234 several weeks and was not possible given the experimental constraints (Philippe, 2016). But, as
235 we will discuss later, using smaller grains may put stronger or weaker constraints on the
236 detectability of PAHs, depending where their bands are situated relative to the CO_2 ice bands.

237 In addition, we measured one mixture of 1.5% PAH combined with a fine fraction (<25µm) of
238 JSC-Mars 1 Mars simulant as well as this dust alone, as a reference.

239 The sample holder is 4.5 cm in diameter and 2 cm deep and has a total volume of 31.8 cm^3.
240 Knowing the mass of the sample, measured just after filling the holder, and the density of bulk
241 CO_2 ice (1.562 g.cm^{-3}) allowed to estimate the initial density and porosity of the sample, which
242 is simply the fraction of the volume of the sample holder not occupied by CO_2 ice.

243 The percentage of H_2O ice mixed in the CO_2 snow was estimated (with uncertainty +/-20%) by
244 comparison of its 1.5 µm band depth with that of the nearby CO_2 bands (at 1.435 and 1.58 µm)
245 and relative to the spectra of a series of CO_2:H_2O ice mixtures previously measured and
246 modelled (Philippe 2016). The mass fraction of H_2O ice in our samples is mostly of the order of
247 the maximum values determined for the South Polar Cap, 0.08-0.12% (Douté et al. 2007) except
248 in one case (~0.20%) where it exceeds these limits.

249   3.3. Experiment Protocol

250 After introduction of the sample holder containing the PAH-CO_2 ice mixture into the CarboN-IR
251 cell and throughout the experiments, the cell and sample holder temperatures were kept at -
252 100°C. Following initial measurements of the samples, sublimation experiments were conducted
253 by pumping the CO_2 gas into the cell to monitor spectral and detection limit changes with
254 sublimation. Bidirectional reflectance spectra (at single geometry) on both full Vis-NIR and

255   partial spectral ranges were recorded regularly during the sublimation experiment to reflect
256   regions of interest for later comparison to observational results from orbital sensors.

4 Results

258   4.1. Preliminary Measurements

259   A first guess of the detectability limit for PAHs in CO_2 ice was established with reference to
260   levels detected on other planetary bodies such as Iapetus, 10^{-4} to 10^{-3} g/cm^3 (Cruikshank et al.,
261   2008). This was then tested at room temperature with a ~1% mix of PAH mixture with a
262   transparent powder (alumine) in order to estimate the minimum amount of PAH required for
263   detection within CO_2 ice but outside its absorption bands. From this preliminary experiment, an
264   approximate detection limit of about 0.1% by weight was determined. This experiment also
265   allowed us to define spectral ranges and resolution needed to detect the PAH mixture without
266   interference from CO_2 ice spectra.

267   A spectrum of the 'pure' PAH mixture was also measured between 0.4 and 4.7 µm (at 20 nm
268   sampling) as a reference (grey line in Figure 1). The positions and intensities of the bands are
269   consistent with the reflectance spectra measured at higher spectral resolution up to 2.5 µm for
270   our three PAHs by Izawa et al. (2014), except the 2.24 µm band which is much stronger in our
271   PAH mixture spectrum.

272   Table 1 shows the details of the three CO_2 ice samples discussed in the subsequent sections.

273

274   *Table 1: Sample Details*

| Sample No.	Sample 1	Sample 2	Sample 3
CO_2 Mass in g	31	23.5	30
PAH Mass in mg	32.7	158.1	161.6
Weight percentage of PAH to CO_2 in %	0.10	0.67	0.54
Weight percentage of H_2O to CO_2 in %	~0.12	~0.2	0.08
Weight fraction of PAH relative to H_2O	~0.8	~3.3	6.75
Density in g/cm^3	0.98	0.74	0.94
Porosity in %	38.5	52	40

275

276   4.2. PAH/CO_2 = 0.1% - Sample 1

277   For the first PAH+CO_2 ice sample, an amount of PAH comparable to our pre-estimated detection
278   limit, 0.1%, was used. During this experiment the speed with which the interior chamber was
279   pumped out from the ambient air resulted in water frost particles condensing on the surface of
280   the sample being blown onto the inside of the window, and could not be removed (in the
281   subsequent experiments this was done more slowly and with additional heating of the window to

282   avoid this problem) meaning that water contamination at the surface of CO_2 ice may be stronger
283   in sample 1.

284   Two spectra were obtained from 0.4-3.6 µm with spectral sampling of 20 nm. As the vacuum
285   was very stable, to aid sublimation, a lamp was used to heat the sample surface, at 27 cm
286   distance from the window, resulting in 70W/m^2 equivalent to Mars at noon at 70° lat, achieving
287   a sample sublimation of ~3 mm between two spectra. Upon examination of these spectra it was
288   clear that the PAH feature at 3.29 µm is not observed on the side of the strong and broad 3.1 µm
289   water ice band (the small shoulder at 3.32 µm is due to CO_2 ice), and so the following spectra
290   were taken only between 0.6 and 2.0 µm at 20 nm sampling. Fig. 1 shows the results.

291

292
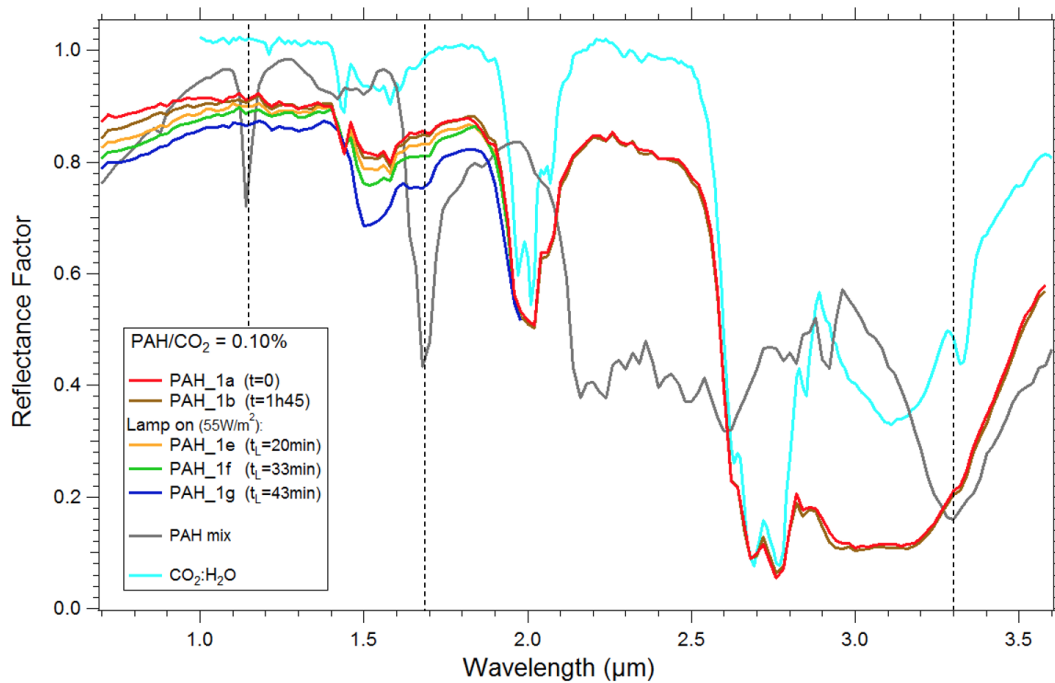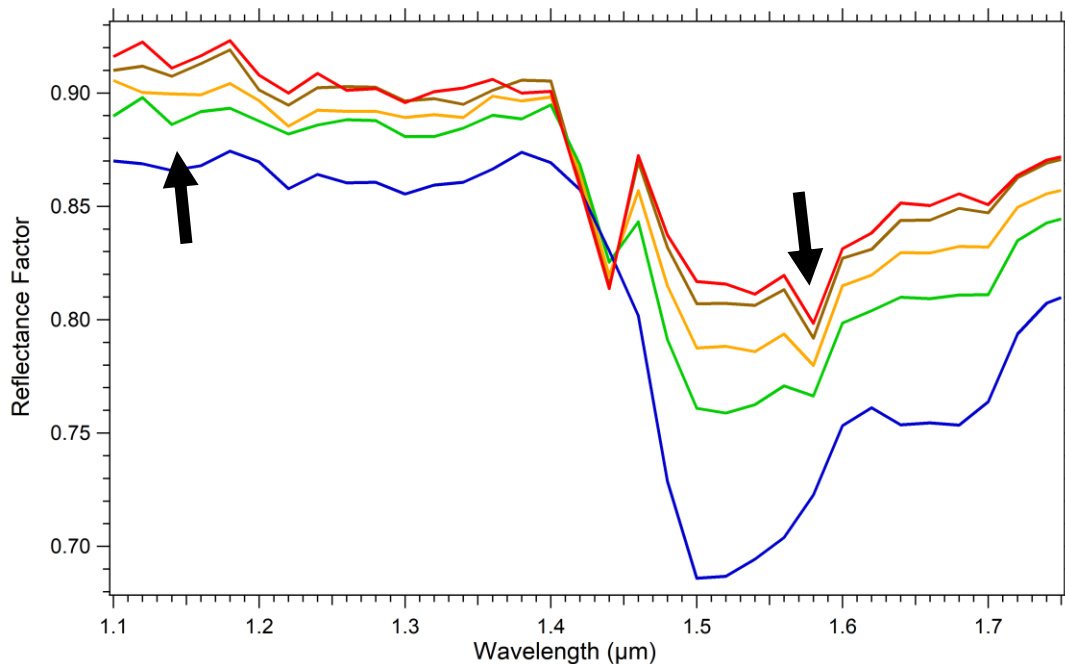
Figure 1: Top: Spectra from sample 1, 0.10% PAH in CO_2 ice (with small amount of H_2O ice ~0.12%) at -100°C during progressive sublimation of CO_2 (PAH_1a to 1g). Black, dotted vertical lines indicate the main infrared PAH absorption features. The sublimation was first free (1a, 1b) then triggered by illumination with a lamp (55W/m^2 at sample surface): 1e-1g. The spectrum of the PAH mix and of CO_2 ice (with small amount of H_2O ice ~0.075%) are also shown for reference. Note the increasing slope below 1.1 µm and the bands at the limit of detection at 1.14 and 1.685 µm. Bottom: Detail of PAH absorption features incicated by black arrows

299   It is clear over time, the overall reflectance of the spectra (PAH1a-1g) decreases as the CO_2 ice
300   sublimates, and the slope increases between 0.7 and 1.1 µm. This is likely to be associated with
301   the steep slope in the corresponding pure PAH mixture spectrum (black line) as sublimation
302   increased the ratio of PAH/CO_2 ice and probably concentrated the PAH at the surface of the
303   sample. We also notice that the water ice feature dominating around 1.52µm increases with
304   sublimation, as the tiny frost particles present at very low level (~0.12%) in CO_2 ice are also
305   segregated at the surface during sample sublimation (Philippe, 2016). A subtle absorption feature
306   with a band depth of about 0.6% is visible in the PAH 1a-1g series of spectra corresponding with
307   the pure PAH feature at 1.14 µm, with another weak feature visible at 1.68 µm (band depth ~
308   1%). This latter band strongly increases in intensity during CO_2 sublimation and reaches an
309   estimated depth of about 3% in the remaining PAH-H_2O ice lag deposit, but at this spectral
310   sampling it is difficult to separate it from the 1.645µm band of H_2O ice. It would seem that the
311   initial 0.10% PAH/CO_2 ice ratio is actually close to the detectability limit at this spectral
312   resolution and sampling, and subsequent experiments used a higher initial ratio and a two times
313   better spectral sampling to confirm the detection of the PAH bands.

314   4.3. PAH/CO_2 = 0.67% - Sample 2

315   For this second experiment, more care was taken to limit frost condensation at the surface of the
316   CO_2 ice sample during transfer to the CarboN-IR cell and the ambient air was pumped more
317   slowly to avoid window condensation or frost particles blown on it, but this was not successful
318   as the water ice bands are about 2 times more intense than in Sample 1 with an estimated amount
319   of H_2O ice of about 0.2%.

320   A higher spectral sampling, 10 nm, was used, meaning it took longer to obtain spectra, so a
321   spectral range of 0.7-2.2 µm was chosen to obtain multiple spectra to observe the evolution of
322   the features at 1.14 and 1.685 µm for the first 4 spectra (PAH2a-PAH2d) during the sublimating
323   sequence. This limitation of the spectral range did not limit this study as CRISM spectra below
324   2.5 µm are the most useful for this work due to the interference of strong atmospheric water and
325   ices features at 2.7-3.3 µm on Mars and because only the lower wavelength PAH features are
326   detected against a background of CO_2 ice. There was a small leak in the cell, increasing
327   sublimation rate, so the lamp was not used for sample 2 to reduce the sublimation rate of CO_2.
328   The spectral range was then increased to 0.7-2.75 µm and left to run overnight, resulting in total
329   of 6 spectra, shown in Fig. 2.

330

331
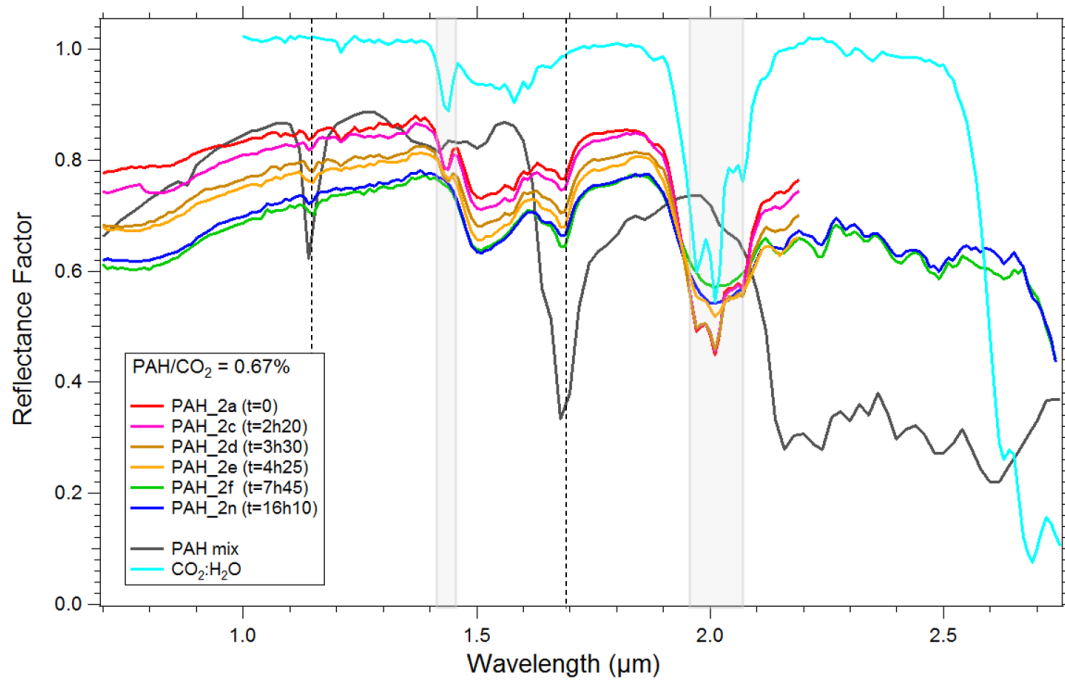
332
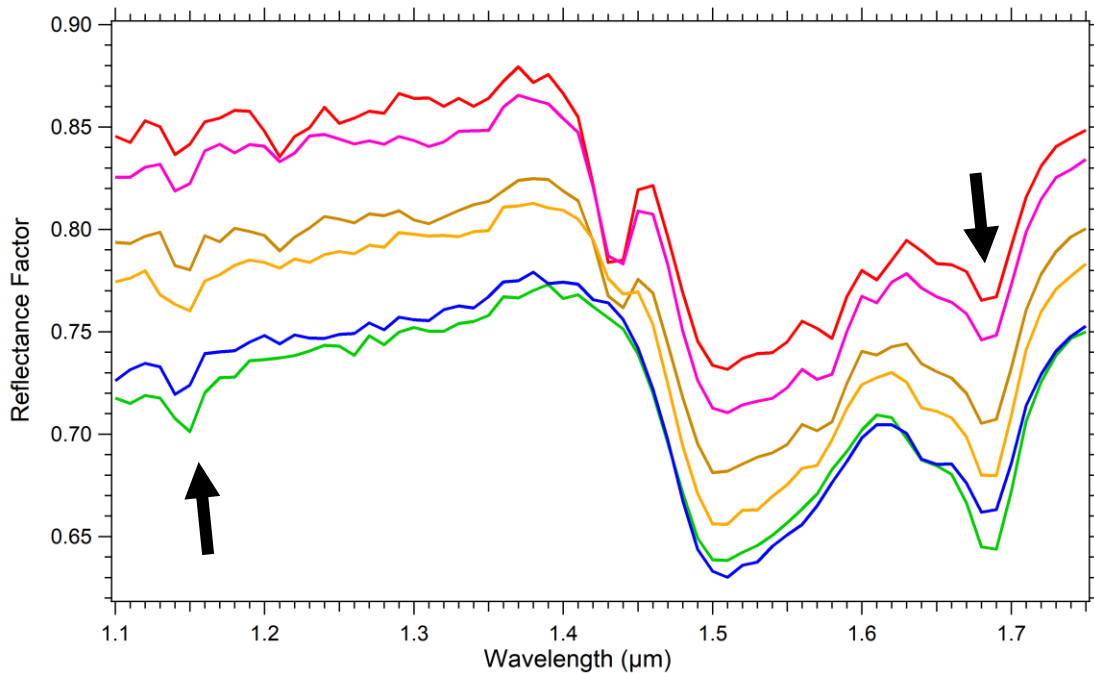
333

334   *Figure 2: Top: Spectra from sample 2, 0.67% PAH in CO_2 ice (with small amount of H_2O ice ~0.2%) at -100°C during*

335   *progressive sublimation of CO_2 (PAH_2a to 2n). Black, dotted vertical lines indicate the main infrared PAH absorption features,*

336   *transparent grey boxes indicate transforming CO_2 ice absorption features. The sublimation was free until the complete*

337   *disappearance of CO_2 ice. The spectrum of the PAH mix and of CO_2 ice (with small amount of H_2O ice ~0.075%) are also shown*

338   *for reference. Note the increasing slope below 1.1 μm and the bands clearly appearing at 1.14 and 1.685 μm, but also in the 2.1-*

339   *2.6 μm range. Bottom: Detail of PAH absorption features incicated by black arrows*

340   With the increased amount of PAH in the ice, the absorption features at 1.14 and 1.685 µm (band
341   depths of 2% and 7% in the mixture, respectively) are now clearly visible throughout all
342   PAH/CO_2 ice spectra, as well as the slope at 0.7-1.1 µm. In the extended spectra PAH2e-PAH2p,
343   there are also corresponding features visible at 2.15, 2.24, 2.29, 2.33, 2.41, 2.49 and 2.62 µm in
344   pure PAH and PAH/CO_2 ice spectra. It is also clear that with the increased initial amount of
345   H_2O ice in this sample (~0.2%, instead of ~0.12% in Sample 1) the CO_2 ice absorption feature at
346   1.435 µm and its triplet features around 2 µm become more rapidly dominated by the strong
347   and broad 1.5 and 2 µm absorption bands of water ice, as CO_2 ice sublimates. When all the CO_2
348   ice has sublimated, leaving only a thin deposit (~170 µm) of water ice-dust mixture, the intensity
349   of both the 1.14 and 1.685 µm bands have increased by about 70%, and then started to decrease
350   slowly while the H_2O ice band was stable.

351

352   4.4. PAH/CO_2 = 0.54% - Sample 3

353   For this experiment a spectral range of 0.4 -2.75 µm was chosen with resolution of 10nm. Details
354   of sample 3 are shown in table 1. This time with an improved preparation protocol we succeeded
355   in efficiently suppressing any additional condensation of frost at the surface of the CO_2 ice, and
356   the water ice content (0.08%) is now similar to what was previously achieved for pure CO_2 ice,
357   as witnessed by the almost identical ratio between the 1.52 µm band of H_2O and 1.435 µm band
358   of CO_2 ice in the initial spectrum 3a (Figure 3).

359   Sixteen spectra were taken throughout the day and overnight during the sublimation sequence.
360   As with experiment 1, the vacuum was very stable, and slow sublimation occurred, resulting in
361   fairly homogenous spectra. Results are shown in Fig. 3.
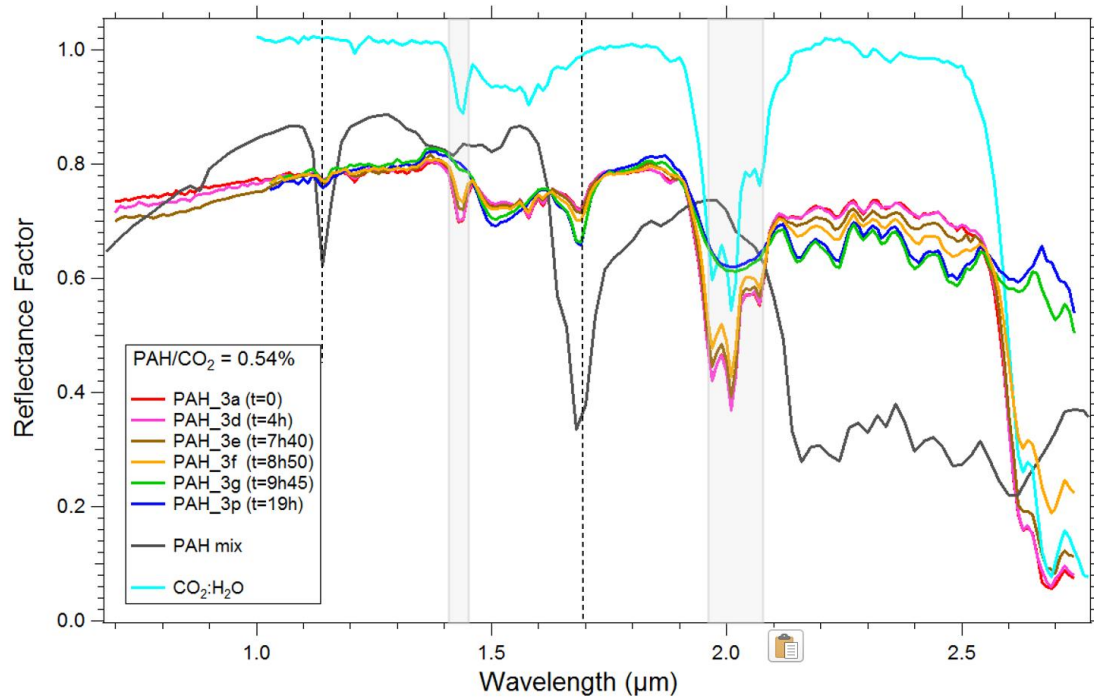
362
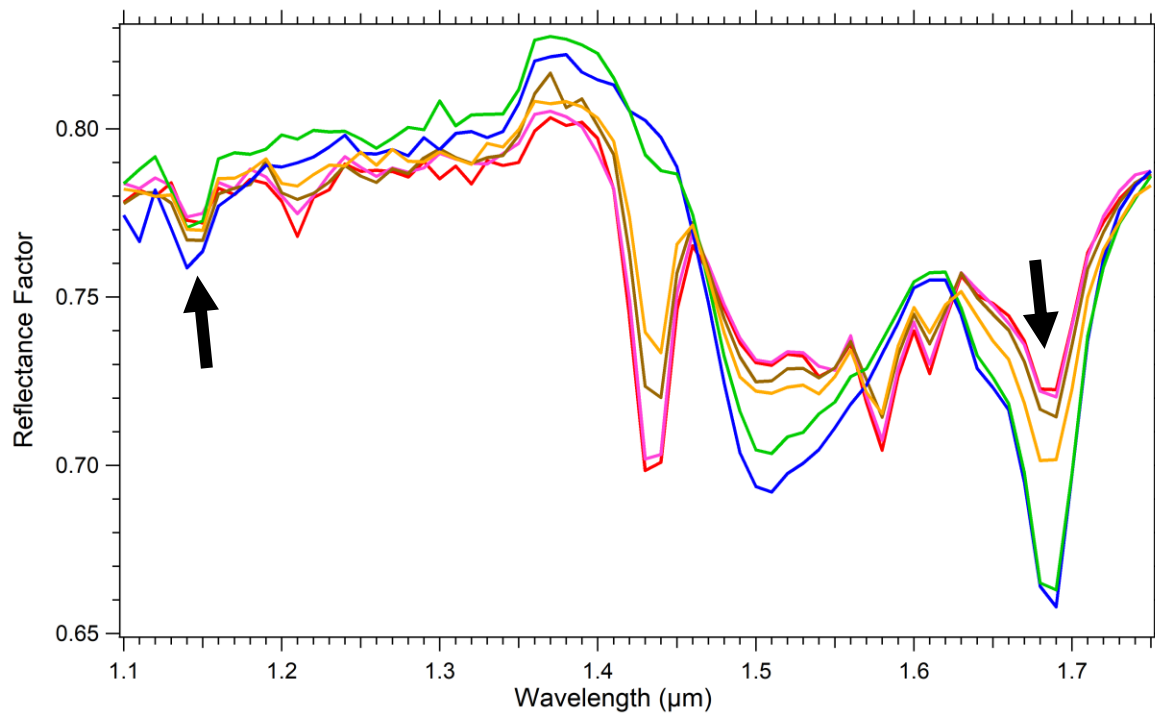
363

364   *Figure 3: Top: Spectra from sample 3, 0.54% PAH in CO_2 ice (with small amount of H_2O ice ~0.08%) at -100°C during*

365   *progressive sublimation of CO_2 (PAH_3a to 3p). Black, dotted vertical lines indicate the main infrared PAH absorption features,*

366   *transparent grey boxes indicate CO_2 ice absorption features mentioned in the text. The sublimation was free until complete*

367   *disappearance of CO_2 ice. The spectrum of the PAH mix and of CO_2 ice (with small amount of H_2O ice ~0.075%) are also shown*

368   *for reference. Note the increasing slope below 1.1 μm and the bands clearly appearing at 1.14 and 1.685 μm, but also in the 2.1-*

369   *2.6 μm range. Bottom: Detail of PAH absorption features inicated by black arrows.*

370

371 With 0.54% PAH, the features at 1.14, 1.685, 2.15, 2.24, 2.41, 2.49 and 2.62 µm are visible as
372 with sample 2. With these higher signal-to-noise spectra, it is also possible to better observe the
373 replicated PAH features at 2.29 and 2.33µm, with the PAH/CO_2 ice mixture between 2.1 and
374 2.5µm closely mirroring the shape of the spectrum for pure PAH mixture. The change in the
375 slope at 0.7-1.1 µm is also clear but unfortunately was not monitored until the end of the
376 experiment. Again as with Sample 2, the CO_2 ice absorption feature at 1.435 µm becomes muted
377 with sublimation, but the triplet feature at ~2 µm is less affected in the first stages of sublimation
378 with an initial 'contamination' of only 0.08% water ice, as was the case with the small amount
379 of H_2O ice in Sample 1. During CO_2 sublimation, the intensity of the 1.14 µm band increased by
380 about 50%, and that of the 1.685 µm by a factor of 2.3 when only a H_2O ice-dust sublimation
381 residue remained at the bottom of the sample holder (only about 120 µm thick). Other bands,
382 such as those of 1.155 µm and 2.49 µm, increased by an even greater proportion.

383

384   4.5. PAH/dust = 1.52% and dust - Samples 4 and 5

385 A final experiment, with two spectra ranging from 0.4-3.9 µm at a resolution of 10nm, was taken
386 of the PAH mixture in Mars simulant JSC Mars-1, weathered volcanic ash from Hawaii (Allen et
387 al., 1998), as well as a pure dust spectrum for reference (Figure 4). The JSC Mars-1 regolith
388 simulant was previously ground and sieved below 25 µm to simulate Martian atmospheric dust.
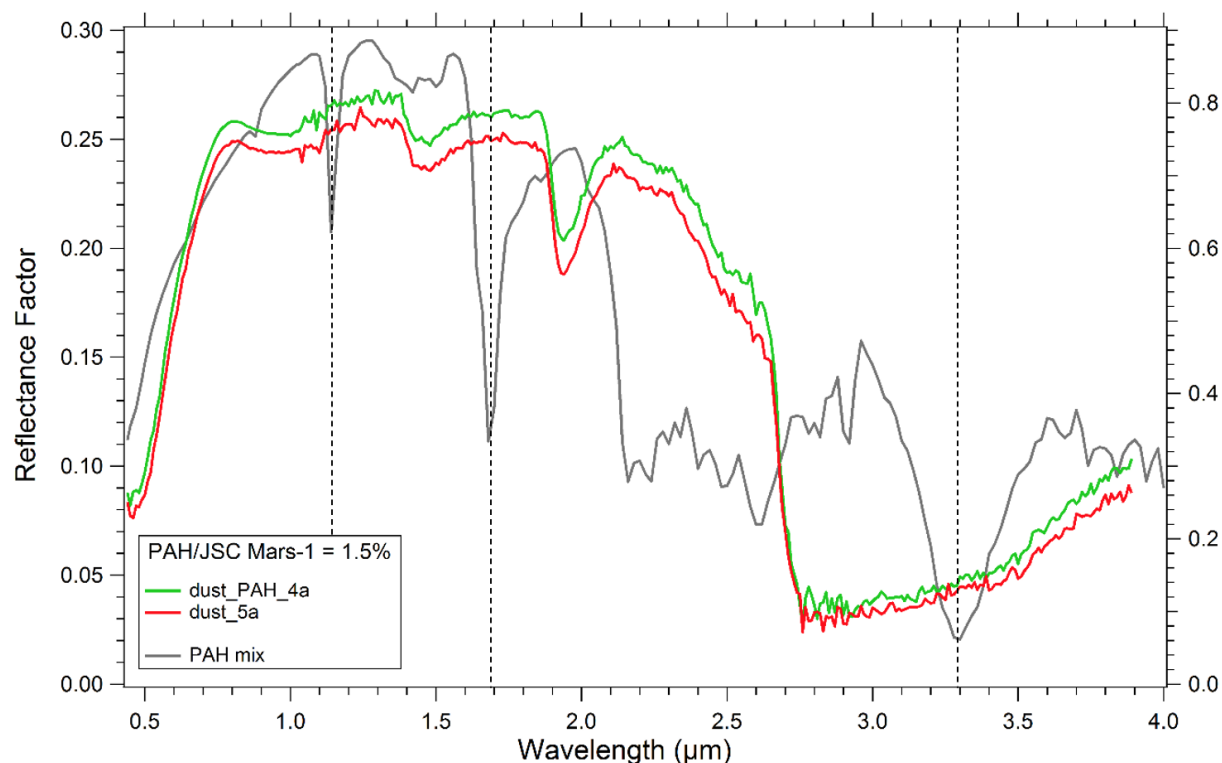389 Sample details are shown in Table 2.

390

391

392 *Table 2: Details of Samples 4 and 5*

Sample Description	Sample 4 : PAH/ JSC Mars-1 Dust Mix	Sample 5: JSC Mars-1 Dust
Dust Mass in g	7.7	15.4
PAH Mass in mg	117	-
Weight percentage of PAH to dust in %	1.52	-
Density in g/cm^3	1.895	1.91
Porosity in %	48.1	49.3

393

394

Figure 4: Spectra from samples 4 and 5, 1.52% PAH in JSC Mars-1 (dust_PAH_4a), and JSC Mars-1 (dust_5a) at room

temperature. Black, dotted vertical lines indicate the main infrared PAH absorption features. The spectrum of the PAH mix is

also shown for reference (right scale). Note that no sign of increase of slope below 1.1 μm and no bands are detected at 1.14,

1.685 μm, nor at 3.29 μm,

Despite PAH particles being clearly visible in the physical sample, and the ratio of PAH to substrate being 2.5 to 3 times higher than in ice samples 2 and 3, (1.52% compared to 0.67% and 0.54%), no spectral features of PAHs were detectable in the dust spectrum.

Other than the pure dust sample being slightly lower in overall reflectance, there is no observable difference in spectra between pure dust and PAH/dust mix. This is most likely because of the relative opacity of dust compared with CO_2 ice, its continuum reflectance being three times lower. If PAHs are not discernible in Martian dust at concentrations an order of magnitude higher than that detected on Iapetus, it is likely to be an extremely limiting factor in detecting PAHs on the SPRC if any potential PAHs are mixed with dust and not in pure form. No known segregation process can concentrate PAH in dust as is the case with PAH/CO_2 ice mixtures. In order to ascertain whether PAHs in small amounts of dust are detectable when mixed in CO_2 ice, further experiments will need to be carried out to better emulate the scarp wall dust deposits in SCT. However, with our current set of experiments, it is already possible to make some

412 extrapolations on the detectability of PAH in materials with different compositions encountered
413 on the South polar cap and in the water ice-dust lag deposits at its margins.

414 **5 Discussion**

415 The results of these novel experiments are extremely useful to allow a future new analysis of
416 orbital observations from the CRISM instrument on Mars Reconnaissance Orbiter, and establish
417 a detection limit for PAHs in CO_2 ice and in H_2O ice-dust lag deposits, not only at the poles, but
418 in shadowed regions elsewhere, in sub-surface ice that may be sampled during future exploration
419 missions as well as on icy bodies. In addition, we ascertained the limitations of observing PAHs
420 directly in 'dry' Martian regolith, a first step towards establishing the detectabililty of PAH in the
421 regolith of other planets. This study also provides more relevant bi-directional reflectance data in
422 the near-infrared range on diagnostic PAH signatures of astrobiological importance to Mars, that
423 are pertinent to planetary ices, as most previous literature, except Izawa et al. (2014), used mid-
424 infrared transmission data from the 1990s which is more relevant to interstellar dust cloud PAH
425 detection.

426 PAHs are extrememly important to theories of abiogenesis, and while their presence is
427 ubiquitous in space, their detection on planetary bodies remains a major objective in planetary
428 science. The attempt to detect them on Mars is worthwhile given the recent discoveries of other
429 organic compounds and subterranean lakes (Freissinet et al., 2015; Ojha et al., 2015; Orosei et
430 al., 2018).

431 In the spectrum of our mixture of three PAHs the strong 1.685 µm band is the first overtone
432 ($2\nu_{CH}$) of the fundamental aromatic symmetric C-H stretch modes (ν_{CH}) occurring at ~3.29 µm.
433 From the position of these two bands, we deduce that the 1.14 µm band is the second overtone
434 ($3\nu_{CH}$) of these modes, and the weak band at 0.88 µm is the third overtone ($4\nu_{CH}$) (Izawa et al.
435 2014). The other bands between 2.1 and 2.9 µm are mostly combination bands between these
436 stretching modes and various types of aromatic C=C deformation modes and C-H stretching and
437 bending modes. Due to the use of phenanthrene-d10 in our sample there are also additional bands
438 at 2.24 and 1.50 µm due to the first and second overtone of the fundamental C-D stretch modes.
439 Weaker bands between 1.30 and 1.55µm are higher order combinations (Izawa et al. 2014). In
440 our discussion we will only consider the 1.14 and 2.685 µm C-H stretch overtone bands.

441 5.1 Detectiability of PAH in CO_2 ice

442 We have shown that the most interesting and sensitive signature of PAH for detection on the
443 Mars residual CO_2 ice cap is this $2\nu_{CH}$ band at 1.685 µm, well outside the CO_2 ice bands and the
444 strongest H_2O ice bands (Figure 6). The only band that can slightly interfere with this PAH band
445 is the 1.645 µm band of water ice, which is seen in our spectra as a weak shoulder on the low
446 wavelength side of the PAH band (see e.g. Figure 2). However, it is shifted to lower
447 wavelengths by 0.04 µm, well above the resolution of all current and future near-infrared
448 spectrometers. We found that even with more than 0.1% water in CO_2 ice, which is rarely the
449 case in the very dry southern hemisphere (Douté et al. 2007 found 0.02-0.12% H_2O in CO_2 ice),
450 this ice band did not preclude the detection of PAH homogeneously mixed at levels below 0.1%
451 in CO_2 ice.

452
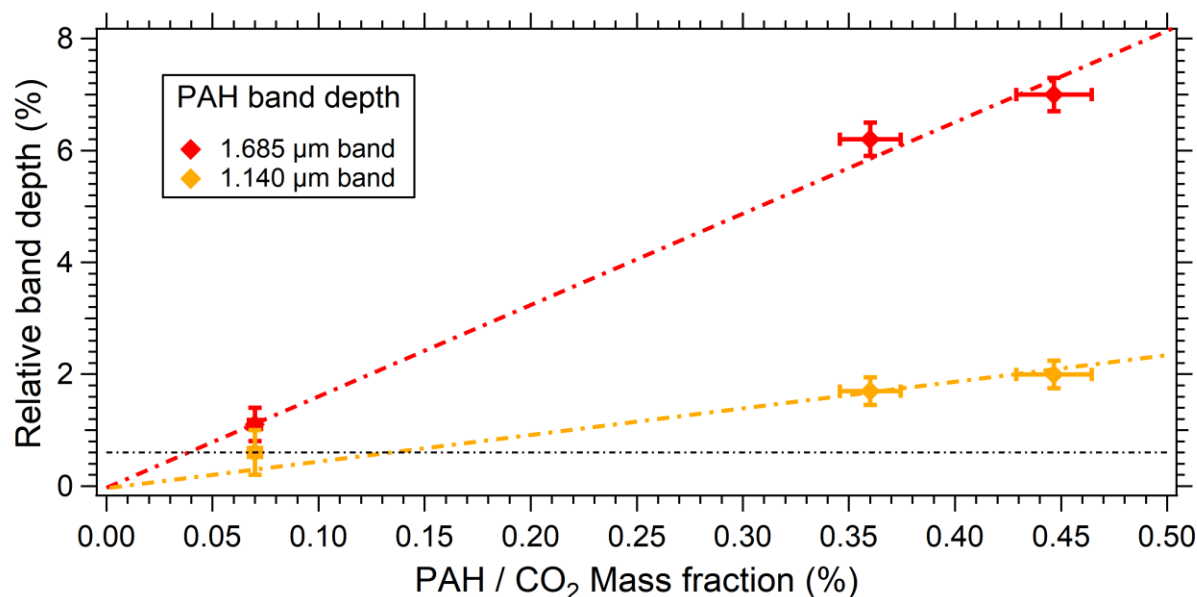
Figure 5: Relative band depth of the 1.14 and 1.685 µm bands of PAH versus the mass fraction of PAH (contributing to these
453

aromatic C-H stretching bands) of the initial homogeneous mixture in CO₂ ice at -100°C. The horizontal line represents a band
454

depth detection level of 0.6% (at 3σ with S/N=450-500).
455

456 In order to better assess the detectability level of this band and the 1.14 µm one for PAH
457 homogeneously mixed with CO_2 ice (before any sublimation), we have plotted in Figure 5 the
458 initial relative band depth of both bands versus the mass fraction of PAH containing C-H bonds
459 (removing phenanthrene-d10 which did not contribute to these bands). Assuming the pre-flight
460 SNR value of 450-500 around 1.14 and 1.68µm given for CRISM (Murchie et al., 2007, Fig.
461 33b), the detection level of these bands in an observed spectrum with reflectance close to 1 (as
462 for CO_2 ice) is for a band depth of 0.6% relative to the nearby continuum (i.e. for a 3σ detection
463 level, horizontal dotted line in figure 5). The detectability of the 1.685 µm band of PAH well
464 mixed in fine grained CO_2 ice (D ~150 µm) is thus at about 0.04% PAH weight fraction, and that
465 of the 1.14 µm at about 0.13%. The detection level for the 1.685 µm band should be only slightly
466 affected at the lower temperature of the SPC (~-150°C), whereas the 1.645 µm H_2O band gets
467 stronger and shifts slightly towards the PAH band (see Fig 2 of Grundy and Schmitt, 1997;
468 1998). The 1.14 µm band is weaker but, on the other hand, absorbs at a wavelength without CO_2
469 absorption and between two much weaker water ice bands.

470 The slope between 0.7 and 1.1 µm, and the absorption features in the 2.1-2.5 µm range may also
471 provide additional clues to confirm detection. The visible slope of PAH occurs in a range of full
472 transparency of both ices, but it cannot be used as a detection criteria as it may be confused with
473 the slope induced by a small amount of contaminating reddish dust. The bands between 2.1 and
474 2.5 µm are also mostly outside any strong CO_2 absorption and are clearly observed in most of
475 our spectra, down to a PAH abundance at 0.1% level, despite a larger abundance of H_2O ice in
476 our samples compared to the Mars South Polar Cap. However, the two generally weak CO_2 ice

477 bands at 2.295 and 2.35 µm may become much stronger in some situations (larger grain size, see
478 e.g. Douté et al. 2007; Langevin et al. 2007) and strongly interfere with this set of PAH bands.

479 On the other hand, the 'classical' strong 3.29 µm fundamental band of PAH interferes with the
480 relatively strong 3.32 µm band of CO_2 ice but is also buried in the wing of the strong water ice
481 band at 3.1 µm which can saturate even with a very small amount (<< 0.1%) of H_2O trapped in
482 CO_2 ice (see e.g. Figure 1). Similarly, when mixed with martian soil this band falls in the wing of
483 the very strong band of both structural and adsorbed H_2O. This 3.29 µm band thus cannot be
484 used to detect PAH in reflectance spectra of icy surfaces.

485 An important point to consider here is the difference in CO_2 ice grain sizes between our samples
486 (~150 µm) and the perennial cap: from several centimetres (clear compact slab) decreasing down
487 to a few millimeters during sublimation in spring (Langevin et al. 2006, Douté et al. 2007).
488 Larger grains increase the intensity of the CO_2 absorption bands and can efficiently hide any
489 other signatures there on in their wings, but on the other hand, such large grains allow light to
490 penetrate and probe much deeper in the wavelength ranges outside the relatively narrow CO_2
491 bands. In particular, the 1.685 µm PAH band is situated at a wavelength where the absorption
492 coefficient of CO_2 is extremely low (< 3 10^{-4} cm^{-1}; Quirico and Schmitt 2004, Hansen 2005). So
493 it is anticipated from radiative transfer considerations that the detection level of this PAH band
494 should be largely improved in such coarse grained or slab ice, possibly down to the 0.01% level.
495 The main limitation will come from the abundance of water ice which has an absorption
496 coefficient around 10 cm^{-1} at 1.685 µm (in the wing of the 1.645 µm H_2O band) for pure ice
497 (Grundy and Schmitt, 1997; 1998), i.e. about 4 orders of magnitude above that of CO_2 ice. A
498 water ice abundance above a few percent should preclude the detection of trace amounts of PAH
499 at this wavelength. On the other hand the 1.14 µm band is situated at a wavelength of minimum
500 absorption of H_2O ice (~ 5 10^{-2} cm^{-1}) and may be a better probe where H_2O ice is moderately
501 abundant.

502 Also, as CO_2 ice sublimates, the PAH contained in the sublimated layers segregates at its surface
503 together with H_2O ice and its band depth progressively increases by a factor which depends on
504 the initial amount of H_2O ice. This increase is only by a factor of 1.55 when the H_2O/CO_2 ratio is
505 large, as for sample 2 (0.20%), but can reach a factor of 2.3 when this ratio is small, as for
506 sample 3 (0.08%). So the 'visibility' of PAH is increased by the CO_2 sublimation only until a
507 mix of PAH and H_2O ice remains. On Mars the accumulation factor of PAH at the surface (at the
508 same initial concentration) will be larger as the thickness of sublimated CO_2 is more than an
509 order of magnitude larger than for our sample (2 cm).

510

511   5.2 Detectability in the PAH-H_2O ice lag deposit

512 Another important result is that for all our samples, the PAH bands are still observed in the H_2O-
513 PAH mixture left over after complete sublimation of the CO_2 ice, and with an increased intensity
514 despite the relatively high initial content in H_2O ice (0.08-0.20%) relative to the Mars South
515 Polar Cap. Our three resulting sublimation lag deposits have H_2O/PAH ratios ranging from 15 to
516 120% (see Table 1) and display very clear and strong PAH bands at all wavelengths for Samples
517 2 and 3 (Figures 2 and 3). Even for Sample 1, where H_2O ice dominates the composition of the

518 mixture, the 1.685 µm is easily detectable, although blended with the 1.645 µm H_2O band (but
519 the sampling was only 20 nm for this sample) which now has a similar intensity (see the blue
520 curve in figure 1). Its relative band depth is about 3%. So PAH may still be detectable in the lag
521 deposit, as a shoulder ~1% deep on the side of the 1.645 µm band, if the initial weight abundance
522 of PAH relative to H_2O ice is more than about 25% (~3 times less than for Sample 1). Given the
523 average concentration of 0.02-0.04% for H_2O ice in CO_2 ice determined for the dry ice-rich
524 terrains (Douté et al. 2007) at Ls~140°, we can still expect to be able to detect PAH mixed with
525 pure H_2O ice in the sublimation lag deposit when PAH is present in the initial CO_2 ice down to a
526 concentration as low as 0.005-0.01%.

527 In our experiment, we did not find a good correlation between the PAH band depths and the
528 PAH/H_2O ice weight ratio, but rather some correlation with the PAH mass column in the sample
529 (Figure 6). This is probably due to the fact that this lag deposit is very thin (65-170 µm,
530 assuming a porosity of 50%) and thus probably still optically thin in these bands. In our
531 experiments a mass column of 0.3 mg/cm^2 may be derived as the 0.6% band depth detection
532 level (for CRISM SNR, see 5.1) for PAH in PAH-H_2O mixtures. However, for optically thick
533 water ice deposits, as on Mars, this may be underestimated. These estimates call for future
534 experiments to measure the actual level of detectability of PAH mixed with water ice.
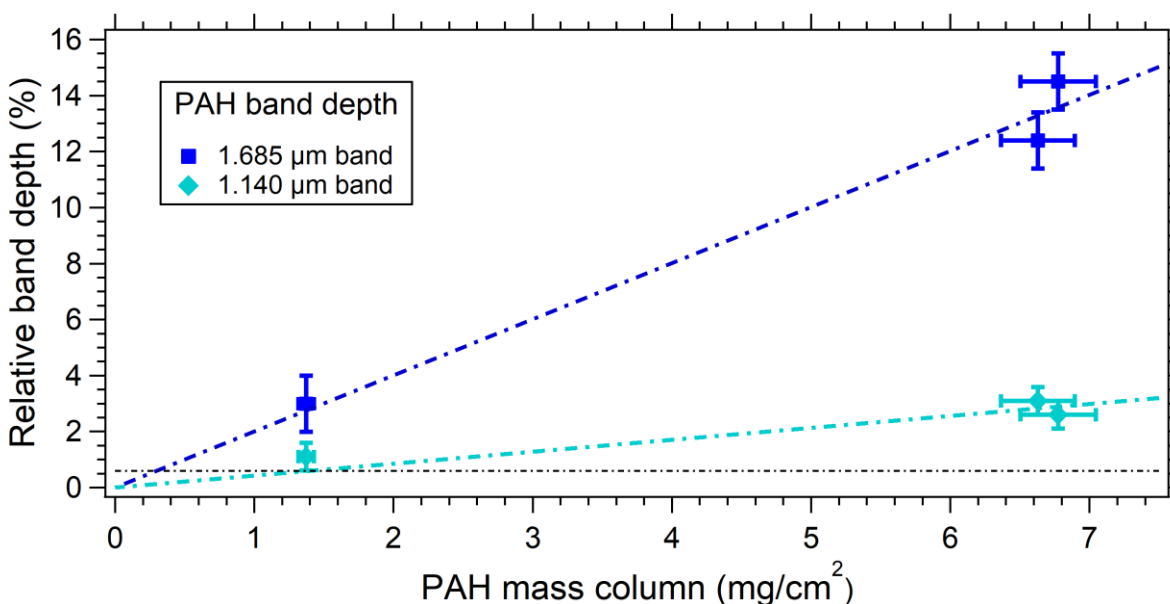
535

536 *Figure 6: Relative band depth of the 1.14 and 1.685 µm bands of PAH versus the mass column of PAH (contributing to these*
537 *aromatic C-H stretching bands) in the PAH-H₂O ice sublimation lag deposit. The horizontal line represents a band depth*
538 *detection level of 0.6% (at 3σ with S/N=450-500).*

539   5.3 Effect of dust on the detectability of PAH

540 As we already saw with our single experiment of PAH-dust mixture, the limitation on the
541 detectability of PAH is also strongly constrained by the amount of dust present in the ice. Indeed
542 the martian dust aerosol particles that are mixed with CO_2 ice have strong absorption coefficients
543 over all the near infrared range (in the range 30-120 cm^{-1} @ 1.14 µm, 50-180 cm^{-1} @ 1.685 µm

544 and increasingly larger above; Douté et al., 2007), so one to three orders of magnitude larger
545 than for H_2O ice and four to six orders larger than for CO_2 ice at the wavelengths of these PAH
546 absorptions. Furthermore, aeolian dust has a much smaller grain size (<10 µm) and therefore, in
547 addition to strongly absorbing light, it will scatter it efficiently and reduce the probed depth. The
548 non-detection of 1.5% PAH in a fine fraction (< 25 µm) of JSCMars-1 analogue is most likely an
549 underestimate of the detection limit of PAHs in dust.

550 On Mars a small amount of dust is mixed with CO_2 ice on the South Polar Cap. Its concentration
551 has been estimated in the 0.02-0.14% range with a dust/H_2O ratio ranging between 0.5 and 4 in
552 the CO_2 ice-rich terrains (Douté et al. 2007). These authors also derived very similar dust/H_2O
553 ratios for the water ice-rich terrains on the margins of the cap, as expected after sublimation of
554 the CO_2 ice.

555 Considering the similarity in absorption coefficient between dust and the strong absorption peak
556 at 2µm of H_2O ice (~100 cm^{-1}), a high abundance of dust (~0.14%) mixed with CO_2 ice will
557 certainly cancel the positive effect of larger CO_2 grain size and limit the detectability of PAH to
558 a higher level than our measured value of 0.06%, possibly closer to 1%. The reflectance of such
559 types of dusty CO_2 ice is only slightly larger (by ~30%) than for the surrounding 'dry' terrains
560 (Douté et al. 2007). So penetration of light is already quite limited. But if dust is present in lower
561 amounts (~0.02-0.04%, reflectance almost twice that of dust) the penetration depth of light in
562 slab CO_2 ice should allow a lower detection limit for PAHs.

563 In the PAH-H_2O-dust sublimation lag deposit a similar degradation of the detection level should
564 occur depending on the dust/ H_2O ratio. If it is at its lower limit (~0.3) the effect should be
565 mostly to reduce the reflectance in the continuum absorption and thus reduce the detectability of
566 the 1.14 µm band and significantly affect the visible slope, but this will only partly reduce the
567 relative band depth of the 1.685 µm band. For higher concentrations of dust relative to both CO_2
568 and H_2O ice, its effect is likely to strongly reduce the detection level of PAH, possibly up to ~1%
569 for the largest observed dust/H_2O ratio ~4 (Douté et al. 2007).

570 All these results and rough estimates based on relative values of absorption coefficients call for
571 experiments to directly measure the detectability of PAHs in mixtures of PAH/dust/H_2O ice
572 dispersed in small amounts in slab CO_2 ice and as sublimation lags in order to better assess both
573 the boosting effect of large CO_2 grain size and the deleterious effects of dust. Radiative transfer
574 models may also help us to understand the detection limits both in experiments and in
575 observations.

576   5.4 Extrapolation to other PAHs

577 Another important question now arises about the wider applicability of our experiments with a
578 selection of only three of the simplest PAHs in comparison to other more complex molecules in
579 this family.

580 It is established that in PAHs the symmetric C-H stretching modes are of two types (for 'bay'
581 and 'non-bay' hydrogen atoms; Baushlisher et al; 2009) but are non-specific of the particular
582 PAH molecule (which show only slight wavelength shifts). They occur in all the members of this
583 family but in different proportions depending on the compactness of the PAH, the 'non-bay H

584   being generally dominant (100% in anthracene and pyrene, 80% in phenanthrene). For the
585   fundamental stretching modes, the two bands occur respectively in the 3.205-3.23 µm (bay H)
586   and 3.23-3.28 µm (non-bay H) ranges for the gas phase, and slightly shifted to higher
587   wavelength in the condensed phase. Accordingly, from a study of the visible-near-infrared
588   reflectance spectra of 47 simple and substituted PAHs in the solid state, Izawa et al. (2014)
589   showed that the overtone bands have mostly one major band (as we observed too) and their
590   positions are relatively well constrained in a narrow range: 1.138-1.150 µm for $3\nu_{CH}$ and 1.673-
591   1.690 µm for $2\nu_{CH}$ mode, with a small shoulder in the range 1.645-1.650 µm.

592   Depending on the exact PAH or mixture, its detectability from the $2\nu_{CH}$ 1.685 µm band may
593   therefore be only slightly decreased if the band shifts to the lower limit of its wavelength range
594   (more interference with the 1.645 µm H_2O ice band) but will increase if its peak shifts away
595   from this band. For the $3\nu_{CH}$ band, no effect on detectability is expected as there is no interfering
596   band nearby. All these shifts have no effects for the detectability in dust as the aeolian dust
597   spectrum display no features in these ranges having a quite flat spectrum.

598   Another factor that may affect detectability (by weight %) is the H/C ratio of the molecule or the
599   PAH mixture. In our mixture this ratio is relatively low (0.45) due to the use of one deuterated
600   molecule. It is similar to the values for larger compact PAH molecules, e.g. 0.5 for coronene
601   ($C_{24}H_{12}$), and lower than for the small PAHs found in Martian meteorites (Becker et al., 1997):
602   0.6 for chrysene ($C_{18}H_{12}$), 0.625 for pyrene ($C_{16}H_{10}$), 0.67 for perylene ($C_{20}H_{12}$) and 0.71 for
603   both anthracene and phenathrene ($C_{14}H_{10}$). But these differences are quite small compared to the
604   previously discussed radiative transfer effects controlling the detectability of PAHs.

605   Only if some aromatic C=C bonds in the PAH material are eliminated, either by substitution (by
606   oxygen atoms, OH, CH_3, …) or by hydrogenation, will the number of aromatic C-H stretching
607   modes decrease, and consequently the strength of both the 1.14 and 1.685 µm bands. In the last
608   case (H_n-PAHs) new, intrinsically stronger, aliphatic C-H stretching modes will appear at higher
609   wavelength, shifted by +0.10-0.26 µm for the fundamental modes (Sandford et al. 2013) and thus
610   by about +0.05-0.13 µm for the first overtone, and + 0.03-0.09 µm for the the second, as
611   observed by Izawa et al. (2014). Their first overtone will be easier to observe as it will shift
612   towards the minimum absorption between the 1.645 µm and the broad 2-µm water ice bands, but
613   it will be the reverse for the second overtone as it will shift in the wing towards the peak
614   absorption of the 1.26 µm H_2O band. However, this particular family of PAH molecules has not
615   been studied in our experiments.

616   **6 Conclusions**

617

618   To summarise: a detectability limit of ~0.04% has been established for observing PAH features
619   in sublimating CO_2 ice but this detection limit may drop by a large factor (to ~0.01%) in coarse
620   grained ice if the amount of dust is at its lowest values (~0.02%) measured on the South Polar
621   Cap. On the other hand, even at its maximum detected concentration in CO_2 ice (~0.12%), water
622   ice should have only a limited effect on the detectability of PAHs.

623

624   Similarly in the PAH-H_2O-dust lag deposits observed on the SPC margins and rim scarps the
625   amount of dust is the main factor that may strongly limit the detectability of PAH (up to only 1%

626   in the original CO_2 ice) while in dust-poor PAH-H_2O lag deposits PAHs can be detected when
627   the PAH/H_2O ice ratio is larger than 25%, i.e. for initial PAH concentration in CO_2 ice in the
628   range 0.01-0.05 %.

629

630   These detectability limits are roughly applicable to most types of C_nH_n PAHs as the two
631   diagnostic bands only slightly change in position and specific band strength among this PAH
632   family. If other PAH families (substituted, hydrogenated…) are present on Mars or other icy
633   bodies, then specific studies of their mixtures with CO_2 or H_2O ice and dust should be performed
634   to assess their detection limits in specific environments.

635

636   The detectability levels achievable in the near-infrared in favorable conditions on Mars are thus
637   of the same order than the amount detected on other planetary bodies, i.e., 10^{-4} to 10^{-3} g/cm3
638   (Cruikshank et al., 2008). One particular advantage of the near infrared bands may be that they
639   allow us to probe deeper into the surface (up to few millimeters or centimeters for clear CO_2 ice
640   slab) than just the very first microns seen by the 3.29 µm PAH band.

641

642   When future space observations of the SPC are recorded at higher spectral resolution & sampling
643   than our measurements (19 nm/10 nm) the better separation between the relatively narrow 1.685
644   µm PAH band and the 1.645 µm H_2O ice band will further improve the PAH detectability.

645
646
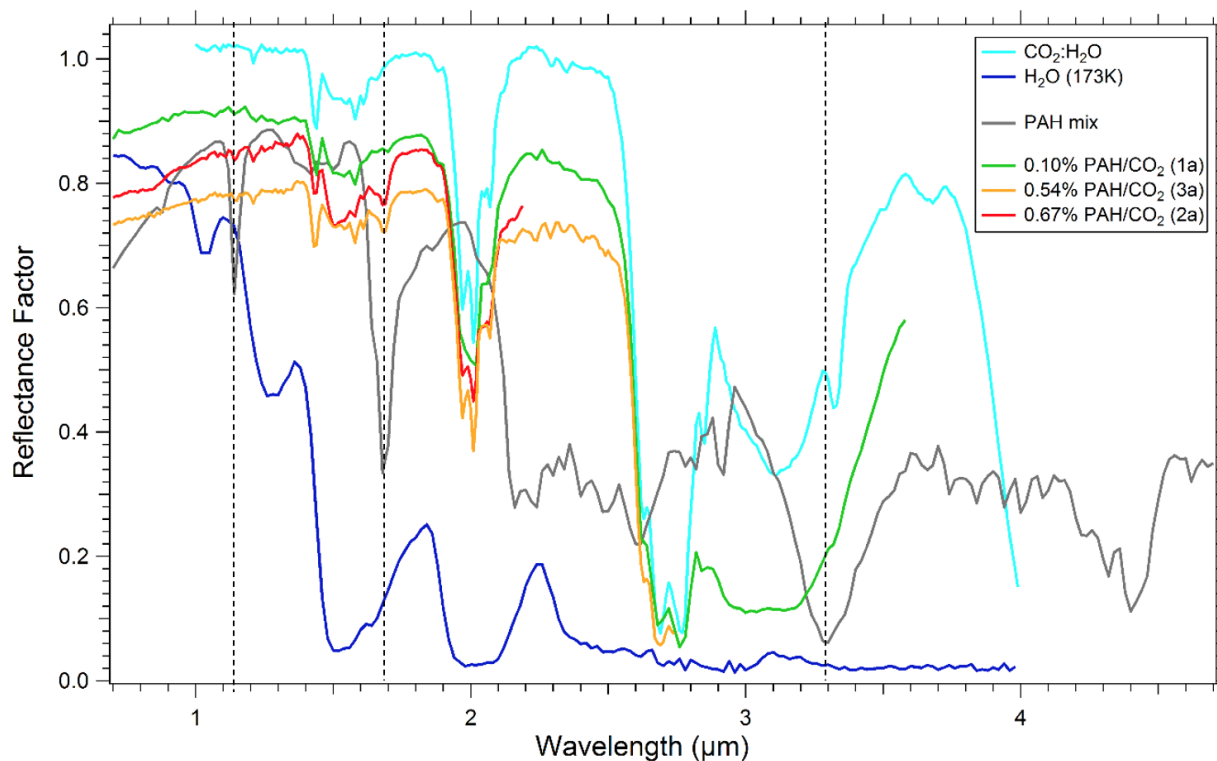
647
648   *Figure 7: Spectra from three initial samples (1a, 2a, 3a) with varying amount of PAH in CO₂ ice (with small amount of H₂O ice*
649   *~0.08-0.2%) compared to the spectrum of the PAH mix and with those of CO₂ ice (with ~0.075% H₂O ice) and pure H₂O ice at*
650   *173K (Philippe 2016). Black, dotted vertical lines indicate the main infrared PAH absorption features.*

651 Analysis of Mars spectra and computer modelling will be carried out in future to apply the
652 empirical laboratory results to CRISM observations, and further laboratory work is planned to
653 obtain PAH spectra pertinent to non-polar regions of Mars. Detectability of PAHs in pure and
654 'contaminated' water ice has far reaching consequences for other planetary bodies such as
655 comets, Europa, Enceladus and Titan, the study of which would greatly benefit from being able
656 to discriminate the effects of PAH and ice on spectra, and comparison with PAH libraries.

References

671 Allamandola, L.J. (2011). *PAHs and Astrobiology*. PAHS and the Universe, EAS publications series, 46. pp.305-317

672 Allen, C.C.; Morris, R.V.; Jager, K.M.; Golden, D.C.; Lindstron, D.J.; Lindstrom, M.M.; Lockwood. J.P. (1998).

673 *Martian Regolith Simulant JSC Mars-1*. Lunar and Planetary Sciences XXIX.

674 Bauschlicher Jr., C. W., E. Peeters, and L. J. Allamandola (2009). *The infrared spectra of very large irregular*

675 *polycyclic aromatic hydrocarbons (PAHs): observational probes of astronomical pah geometry, size, and charge.* The

676 Astrophysical Journal, 697:311–327,Becker L., Glavin D.P., Bada J.F. (1997). *Polycyclic aromatic hydrocarbons*

677 *(PAHs) in Antarctic Martian meteorites, carbonaceous chondrites, and polar ice*. Geochimica et Cosmochimica Acta,

678 61, pp. 475-481.

679 Benner, S.A., Devine, K.G., Matveeva, L.N. and Powell, D.H., (2000). *The missing organic molecules on*

680 *Mars.* Proceedings of the National Academy of Sciences, *97*(6), pp.2425-2430.

681 Bonnefoy N., Brissaud O., Schmitt B., Douté S., Fily M., Grundy W., Rabou P. (2000). *Experimental system for the*

682 *study of planetary surface materials - BRDF*. Remote Sensing Reviews, 19, 59-74.

683 Botta O. and Bada J. (2002). *Extraterrestrial organic compounds in meteorites*. Surveys in Geophysics 23, pp.411–

684 467.

685 Brissaud O., Schmitt B., Bonnefoy N., Douté S., Rabou P., Grundy W., Fily M. (2004). *Spectrogonio radiometer for*

686 *the study of the bidirectional reflectance and polarization functions of planetary surfaces.* Applied Optics 43, No. 9.

687 Byrne, S. (2009). *The Polar Deposits of Mars*. Annual Review of Earth and Planetary Science, 37. pp.535-560

688 Campbell, Jacqueline; Schmitt, Bernard; Beck, Pierre; Brissaud, Olivier (2017): *Vis-NIR reflectance spectra of a mix*
689 *of three PAHs, PAHs mixed with CO₂ snow and PAHs mixed with JSC Mars-1 simulant*. SSHADE/CSS (OSUG Data
690 Center). Dataset/Spectral Data. doi:10.26302/SSHADE/EXPERIMENT_BS_20181101_001

691 Campbell, J.D., Sidiropoulos, P. and Muller, J.P., 2018. *A search for polycyclic aromatic hydrocarbons over the*
692 *Martian South Polar Residual Cap.* Icarus, 308, pp.61-70.

693 Ceamanos, X., Douté, S., Fernando, J., Schmidt, F., Pinet, P. and Lyapustin, A., 2013. *Surface reflectance of Mars*
694 *observed by CRISM/MRO: 1. Multi-angle Approach for Retrieval of Surface Reflectance from CRISM observations*
695 *(MARS-ReCO)*. Journal of Geophysical Research: Planets, 118(3), pp.514-533.

696 Cockell, C.S. Catling, D.C. Davis, W.L. Snook, K. Kepner, R.L. Lee, P. McKay, C.P. (2000). *The ultraviolet*
697 *environment of Mars: Biological Implications past, present and future*. Icarus. 146. 343-359

698 Colangeli, L. Mennella, V. Baratta, G.A. Bussoletti, E. Strazzulla, G. (1992). *Raman and infrared spectra of polycyclic*
699 *aromatic hydrocarbon molecules of possible astrophysical interest*. The Astrophysical Journal. 396. 369–377.

700 Cruikshank, D.P. Wegryn, E. Dalle Ore, CM. Brown, R.H. Bibring, J-P. Buratti, B.J. Clark, R.N. McCord, T.B.
701 Nicholson, P.D. Pendleton, Y.J. Owen, T.C. Filacchione, G. Coradini, A. Cerroni, P. Capaccioni, F. Jaumann, R.
702 Nelson, R.M. Baines, K.H. Sotin, C. Bellucci, G. Combes, M. Langevin, Y. Sicardy, B. Matson, D.L. Formisano, V.
703 Drossart, P. Mennella, V. (2008). *Hydrocarbons on Saturn's satellites Iapetus and Phoebe*. Icarus. 193. 334-343

704 Cruikshank, D.P. Dalle Ore, C.M. Clark, R.N. Pendleton, Y.J. (2014) *Aromatic and aliphatic organic materials on*
705 *Iapetus: Analysis of Cassini VIMS data*. Icarus. 233. 306-315

706 Dartnell, L.R. Patel, M.R. Storrie-Lombardi, M.C. Ward, J.M. Muller. J.P. (2012). *Experimental determination of*
707 *photostability and fluorescence-based detection of PAHs on the Martian surface*. Meteorics and Planetary Science.
708 47. 5. pp.806-819

709 Douté, S., B. Schmitt, Y. Langevin, J.-P Bibring, F. Altieri, G. Bellucci, B. Gondet, F. Poulet and the MEX OMEGA
710 Team (2007). *South pole of Mars: Nature and composition of the icy terrains from Mars Express OMEGA*
711 *observations.* Planet. Space Science, 55, 113-133.

712 Dullemond, P. Henning, T.H. Visser, R. Geers, V.C. van Dishoeck, E.F. Pontoppidan, K.M. (2007). *Dust*
713 *sedimentation in protoplanetary disks with polycyclic aromatic hydrocarbons.* Astronomy and Astrophysics. 473.
714 457-466

715 Fairén, A.G. Davila, A.F. Lim, D. Bramall, N. Bonaccorsi, R. Zavaleta, J. Uceda, E.R. Stoker, C. Wierzchos, J. Dohm,
716 J.M. Amils, R. Andersen, D. McKay, C.P. (2010). *Astrobiology through the Ages of Mars: The Study of Terrestrial*
717 *Analogues to Understand the Habitability of Mars*. Astrobiology. 10. 8. 821-843

718 Freissinet, C. Glavin, D.P Mahaffy, P. R. Miller, K. E. Eigenbrode, J. L. Summons, R. E. Brunner, A. E. Buch, A.
719 Szopa, C. Archer Jr., P. D. Franz, H. B. Atreya, S. K. Brinckerhoff, W. B. Cabane, M. Coll, P. Conrad, P. G. Des
720 Marais, D. J. Dworkin, J. P. Fairén, A. G. François, P. Grotzinger, J. P. Kashyap, S. ten Kate, I. L. Leshin, L. A.
721 Malespin, C. A. Martin, M. G. Martin. Torres, F. J. McAdam, A. C. Ming, D. W. Navarro-González, R. Pavlov, A.
722 A. Prats, B. D. Squyres, S. W. Steele, A. Stern, J. C. Sumner, D. Y. Sutter, B. Zorzano, M.-P. The MSL Science Team.
723 (2015). *Organic molecules in the Sheepbed Mudstone, Gale Crater, Mars.* Journal of Geophysical Research: Planets.
724 120. 3. 495-514.

Grisolle F. (2013*). Les condensats saisonniers de Mars : étude expérimentale de la formation et du métamorphisme de glaces de CO₂. PhD thesis,* Université Joseph Fourier, Grenoble. [TEL: https://tel.archives-ouvertes.fr/tel-01167247/document]

Herbst, E. van Dishoek, E.F. (2009). *Complex Organic Interstellar Molecules. Annual Review of Astronomy and Astrophysics.* 47. 427-480

Grundy, W.; Schmitt, B. (1997): *NIR Optical constants spectrum of H2O Ih crystal and H2O liquid from 20 to 293 K.* SSHADE/GhoSST (OSUG Data Center). Dataset/Spectral Data. https://doi.org/10.26302/SSHADE/EXPERIMENT_BS_20120924_011.

Grundy, W., and B. Schmitt 1998. *The temperature-dependent near-infrared absorption spectrum of hexagonal H₂O ice*. J. Geophys. Res. E*, **103**,* 25809-25822.

Hansen, G. (2005). *Ultraviolet to near-infrared absorption spectrum of carbon dioxide ice from 0.174 to 1.8 µm.* Journal of Geophysical Research, 110, E11003.

Hecht, M.H., Kounaves, S.P., Quinn, R.C., West, S.J., Young, S.M.M., Ming, D.W., Catling, D.C., Clark, B.C., Boynton, W.V., Hoffman, J. and DeFlores, L.P., (2009). *Detection of perchlorate and the soluble chemistry of Martian soil at the Phoenix lander site.* Science, 325(5936), pp.64-67

Izawa, M.R.M., Applin, D.M., Norman, L. and Cloutis, E.A., (2014). *Reflectance spectroscopy (350–2500 nm) of solid-state polycyclic aromatic hydrocarbons (PAHs).* Icarus, 237, pp.159-181.

Jian, J.J. Ip,W.H. (2009). *Seasonal patterns of condensation and sublimation cycles in the cryptic and non-cryptic regions of the South Pole*. Advances in Space Research. 43. pp.138-142

Langevin,Y., J.-P. Bibring, F. Montmessin, F. Forget, M. Vincendon, S. Douté, F. Poulet, and B. Gondet (2007). *Observations of the south seasonal cap of Mars during recession in 2004–2006 by the OMEGA visible/near-infrared imaging spectrometer on board Mars Express*. Journal of Geophysical Research, 112, E08S12.

Kalpana, M.S., Babu, E.V.S.S.K., Mani, D., Tripathi, R.P. and Bhandari, N., (2021). *Polycyclic aromatic hydrocarbons in the Mukundpura (CM2) Chondrite*. Planetary and Space Science, 198, p.105177.

Klein, H.P., (1978). *The Viking biological experiments on Mars.* Icarus, 34(3), pp.666-674

Li, A. (2008). *PAHs in comets: An overview.* Physics and Astronomy. 53. 31-44. DOI: https://doi.org/10.1007/978-3-540-76959-0_21

Lopez-Puertas, M. Dinelli, B.M. Adriani. A. Funke, B. Garcia-Comas, M. Moriconi, M.L. D'Aversa, E.D. Boersma, C. Allamandola, L.J. (2013). *Large abundances of polycyclic aromatic hydrocarbons in Titan's upper atmosphere*. The Astrophysical Journal. 770.132. 1-8

Malin, M.C. Caplinger, M.A. Davis, S.D. (2001). *Observational evidence for an active surface reservoir of solid carbon dioxide on Mars.* Science. 294. 2146-2148.

McKay D. S., Gibson E. K., Jr., Thomas-Keprta K. L., Vali H., Romanek C. S., Clemett S. J., Chillier X. D. F., Maechling C. R., and Zare R.N. (1996) *Search for past life on Mars: Possible relic biogenic activity in martian meteorite ALH84001*. Science 273, 924-930.

Mulas, G. Malloci, C. Joblin, C. Toublanc, D. (2005). *Estimated IR and phosphorescence emission fluxes for specific Polycyclic Aromatic Hydrocarbons in the Red Rectangle.* Astronomy and Astrophysics. 446. pp.537-549

762   Murchie, S. Arvidson, R. Bedini, P. Beisser, K. Bibring, J-P. Bishop, J. Boldt, J. Cavender, P. Choo, T. Clancy, R.T.

763   Darlington, E.H. Des Marais, D. Espiritu, R. Fort, D. Green, R. Guinness, E. Hayes, J. Hash, C. Heffernan, K.

764   Hemmler, J. Heyler, G. Humm, D. Hutcheson, J. Izenberg, N. Lee, R. Lees, J. Lohr, D. Malaret, E. Martin, T.

765   McGovern, J.A. McGuire, P. Morris, P. Mustard, J. Pelkey, S. Rhodes, E. Robinson, M. Roush, T. Schaefer, E.

766   Seagrave, G. Seelos, F. Silverglate, P. Slavney, S. Smith, M. Shyong, W.J. Strohbehn, K. Taylor, H. Thompson, P.

767   Tossman, B. Wirzburger, M. Wolff, M. (2007). *Compact Reconnaissance Imaging Spectrometer for Mars (CRISM)*

768   *on Mars Reconnaissance Orbiter (MRO).* Journal of Geophysical Research. 112. E05S03, doi:10.1029/2006JE002682

769   Navarro-González, R., Vargas, E., de La Rosa, J., Raga, A.C. and McKay, C.P., (2010). *Reanalysis of the Viking*

770   *results suggests perchlorate and organics at midlatitudes on Mars.* Journal of Geophysical Research: Planets,

771   115(E12)

772   Oberg, K.I. Garrod, R.T. van Dishoek, E.F. Linnartz, H. (2009). *Formation rates of complex organics in UV irradiated*

773   *CH$_3$OH-rich ices*. Astronomy and Astrophysics. 504. 3. 891-913

774   Ojha, L. Willhelm, M.B. Murchie,. S.L. MEwen, S.S. Wray, J.J. Hanley, J. Masse. M. Chojnacki, M. (2015). *Spectral*

775   *evidence for hydrated salts in recurring slope lineae on Mars*. Nature Geoscience. 8. 829-832.

776   Orosei, R. Lauro, S.E. Pettinelli, E. Cicchetti, A. Coradini, M. Cosciotti, B. Di Paulo, F. Flamini, E. Mettei, E.

777   Pajola, M. Soldovieri, F. Cartacci, M. Cassenti, F. Frigeri, A. Giuppi, S. Martufi, R. Masdea, A. Mitri, A. Nenna, C.

778   Noschese, R. Restano, M. Seu, R. (2018). *Radar evidence of subglacial liquid water on Mars*. Science. DOI:

779   10.1126/science.aar7268

780   Philippe S. (2016). *Microphysique des processus saisonniers des glaces de Mars et Pluton : suivi par télédétection*

781   *hyperspectrale et étude expérimentale*. PhD thesis, Université Grenoble Alpes, Grenoble. [TEL: https://tel.archives-

782   ouvertes.fr/tel-01560378/document]

783   Piquex.S. Edwards, C.S. Christensen, P.R. (2008). *Distribution of the ices exposed near the south pole of Mars using*

784   *THEMIS temperature measurements*. Journal of Geophysical Research. 113. E02006

785   Plaxco, K.W. Gross, M. (2011). *Astrobiology: A Brief Introduction*. 2nd Edition. The John Hopkins University Press.

786   pp.145-152

787   Quirico, Eric; Schmitt, Bernard (2004): *Near-IR optical constants of crystalline CO$_2$ ice at 179 K completed with 28K*

788   *data.*   SSHADE/GhoSST   (OSUG   Data   Center).   Dataset/Spectral   Data.

789   https://doi.org/10.26302/SSHADE/EXPERIMENT_BS_20130215_001

790   Sandford, S. A., M. P. Bernstein, and C. K. Materese (2013). *The infrared spectra of polycyclic aromatic hydrocarbons*

791   *with excess peripheral H atoms (Hn-PAHs) and their relation to the 3.4 and 6.9µm PAH emission features*. The

792   Astrophysical Journal Supplement Series, 205:8.

793   Schuerger, A.C and Clark, B.C., (2008). *Viking biology experiments; Lessons learned and the role of ecology in future*

794   *life-detection experiments.* In Strategies of Life Detection (pp. 233-243_. Springer, Boston, MA

795   Smith, M.D., (2004). *Interannual variability in TES atmospheric observations of Mars during 1999–*

796   *2003*. Icarus, 167(1), pp.148-165.

797   Tang N. (2018) PAHs/NPAHs. In: Hayakawa K. (eds) *Polycyclic Aromatic Hydrocarbons*. Springer, Singapore.

798   https://doi.org/10.1007/978-981-10-6775-4_3

799   Thompson, M.S., Morris, R.V., Clemett, S.J., Loeffler, M.J., Trang, D., Keller, L.P., Christoffersen, R. and Agresti,

800   D.G., (2020). *The effect of progressive space weathering on the organic and inorganic components of a*

801   *carbonaceous chondrite*. Icarus, 346, p.113775.

802   Vincent, W.F. Rae, R. Laurion, I. Howard-Willimans, C. Priscu, J.C. (1998). *Transparency of Antarctic ice-covered*

803   *lakes to solar UV radiation.* Limnology and Oceanography. 43. 4. 618-624

804   Wright, I.P., Grady, M.M. and Pillinger, C.T., (1989). *Organic materials in a Martian meteorite*. Nature, 340(6230),

805   pp.220-222.